International Journal of Thermal Sciences 170 (2021) 107156

Contents lists available at ScienceDirect

International Journal of Thermal Sciences

journal homepage: www.elsevier.com/locate/ijts

Theoretical modeling of heat transfer in a multilayer rectangular body with spatially-varying convective heat transfer boundary condition

Long Zhou [a,b], Mohammad Parhizi [b], Ankur Jain [b,*]

[a] School of Mechanical and Power Engineering, Henan Polytechnic University, Jiaozuo, Henan, China
[b] Mechanical and Aerospace Engineering Department, University of Texas at Arlington, Arlington, TX, USA

ARTICLE INFO

Keywords:
Thermal conduction
Multilayer body
Semiconductor thermal management
Theoretical modeling
Jet impingement cooling

ABSTRACT

Theoretical analysis of heat transfer in a multilayer body is relevant for several engineering applications where heat transfer occurs through a stack of thermally dis-similar materials. In most of such literature, a constant convective heat transfer coefficient is assumed as a boundary condition at one end of the body. In contrast, there is a lack of work to model a problem with spatial variation in the convective heat transfer coefficient. This paper presents an analytical solution for thermal conduction in a multilayer rectangular body with spatially varying convective heat transfer coefficient at one end. In addition, this solution also accounts for internal heat generation and inter-layer thermal contact resistance and spatially varying heat flux on the other end of the body. The solution is derived in a series form, and it is shown that the coefficients of the series can be determined by solving a well-defined set of linear algebraic equations. The analytical solution is verified by comparison with numerical simulations, as well as with standard solution for a simplified special case. The impact of spatially varying cooling provided by jet impingement is analyzed using the analytical solution. A resource optimization problem pertaining to the optimal use of jet cooling is solved. Results presented here may benefit thermal management analysis of a broad variety of engineering applications involving heat transfer in multi-layer bodies.

1. Introduction

Thermal conduction in a multilayer body is an important heat transfer problem that occurs in multiple engineering applications [1]. Multilayer heat transfer analysis becomes particularly important when the layers have distinct properties such as thermal conductivity, as well as heat generation rate and thickness. Semiconductor chip packaging is an example of a multilayer engineering system in which heat transfer analysis is important [2]. A metal-based heat spreader is often attached to the Silicon chip with a thin layer of thermal interface material (TIM) for efficient heat spreading, resulting in a multi-layer structure. Further, in the case of low power chips operated without a heat spreader or heat sink, heat transfer through the multi-layer motherboard is important. In more recent electronics technologies, the chip itself may comprise multiple heterogeneous layers. For example, three-dimensional integrated circuits (3D ICs) have been developed that comprise multiple heterogeneous chips bonded to each other to form a vertical stack of chips [3,4]. In each of these cases, heat generated must be conducted through multiple layers before being dissipated at one end, for example, by convective cooling. Due to the non-uniform distribution of heat sources, and the ability to remove heat only from the ends, heat transfer analysis and optimization is critical [5].

Significant literature already exists on the analysis of multilayer heat transfer problems using a variety of analytical methods. The eigenfunction expansion method has been used to solve transient heat conduction problem in a one-dimensional, multi-layer medium [6]. For such problems, non-homogeneous boundary conditions have been handled by decomposing the dimensionless temperature into steady and transient components [7]. Improvements in computational time have been demonstrated through appropriate transformations [8]. Other analytical methods used for solving multilayer problems include Laplace transform method [9], distributed transfer function method [10], finite integral transform method [11,12], and Green's function method [13]. A method using two auxiliary functions related to the quasi-static component of temperature has also been developed [14]. In the specific context of multilayer 3D ICs, iterative [15] and non-iterative [2] analytical expressions for temperature distribution have been derived for the case of convective cooling at one end. The thermal conduction problem in a multilayer body with heating at one end of the body has been discussed [16]. Thermal conduction in a multilayer semiconductor stack with internal heat generation has also been presented [17].

* Corresponding author. 500 W First St, Rm 211, Arlington, TX, 76019, USA.
E-mail address: jaina@uta.edu (A. Jain).

https://doi.org/10.1016/j.ijthermalsci.2021.107156
Received 1 February 2021; Received in revised form 25 May 2021; Accepted 22 June 2021
Available online 9 July 2021

Nomenclature

h	convective heat transfer coefficient (W/m^{2}K)
k	thermal conductivity (W/mK)
M	number of layers
N	number of eigenvalues
Q	surface heat flux (W/m^2)
q	internal heat generation rate (W/m^3)
R	thermal contact resistance (Km^2/W)
T	temperature rise above ambient (K)
x,z	Spatial coordinates (m)

In most papers discussed above, a convective boundary condition is assumed at one end of the multilayer structure. The convective heat transfer coefficient h is commonly considered to be uniform. However, even for highly simplified cases, convective heat transfer coefficient may vary significantly over the cooling surface. For example, even when the cooling face of the multilayer body is being cooled by one of the simplest flow fields – one-dimensional flow past a flat plate – the convective heat transfer coefficient is known to vary with x, and analytical expressions are available for laminar conditions [18]. For more realistic and complicated cooling configurations, such as jet impingement cooling, the convective heat transfer coefficient is expected to be an even stronger function of space. For example, for a circular jet impinging on a surface, the convective heat transfer coefficient is very large close to the site of impingement and reduces rapidly outwards [19]. In modeling such scenarios, the assumption of uniform convective heat transfer coefficient is likely to result in significant error.

While the principle of orthogonality combined with the separation of variables method often easily yields the solution for problems with uniform convective heat transfer coefficient, spatial variation in h makes the problem more complicated. Single-layer problems with spatially varying convective heat transfer coefficient have been solved in the past by considering a large but finite number of eigenvalues and deriving a set of algebraic equations to determine the values of the corresponding coefficients. Using this approach, single-layer thermal conduction problems in fins [20], gas turbine experiments [21], cylinders [22] and spheres [23] have been solved. The problem of thermal conduction in a semiconductor chip with spatially varying convective heat transfer coefficient has also been solved [24] using similar methods, but only for a single-layer chip. In contrast, thermal conduction analysis in a multi-layer body with spatially varying convective heat transfer coefficient has not been sufficiently addressed in the past. Variation of h in space adds significant complexity to this problem, but it is very desirable to address this problem since it more closely models several engineering systems, including multilayer semiconductor chips. Some relevant work exists on multilayer analysis for a cylindrical body [25], however, analysis is needed for addressing problems related to multilayer semiconductor chips that usually have rectangular geometry.

This paper presents an analytical solution for thermal conduction in a multilayer rectangular body with non-uniform heat flux at one end and non-uniform convective heat transfer coefficient at the other end. A general case considering layers of different thicknesses, thermal properties, internal heat generation rates is analyzed. Thermal contact resistance between layers is also accounted for. Expressions for the resulting temperature distribution in the multilayer structure are derived. It is shown that the coefficients appearing in these expressions are given by the solution of a set of algebraic linear equations. Special cases of relevance to heat transfer in semiconductor chips and packaging are discussed. While the equations being solved here may be quite standard, spatial variation in h introduces significant mathematical complexity, as seen in the next section. Results presented here expand our understanding of heat transfer in a multilayer rectangular body, with applications in several engineering systems.

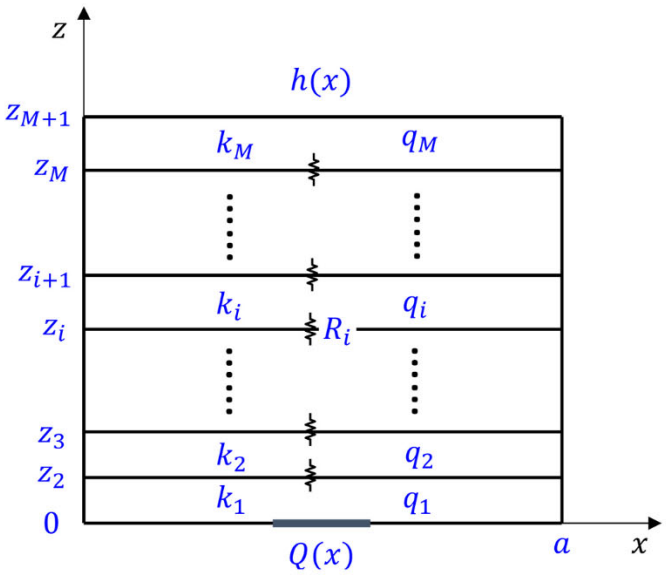

Fig. 1. Schematic of the multilayer geometry considered in this work. Each of the M layers has a distinct thermal conductivity, k_i, internal heat generation rate, q_i, and thickness, z_{i+1}-z_i. A given heat flux $Q(x)$ occurs on the bottom face, and the top face is being convectively cooled with spatially varying heat transfer coefficient $h(x)$.

2. Derivation of analytical solution

This section presents an analytical solution for determining the steady state temperature distribution for a multilayer body with internal heat generation, inter-layer thermal contact resistance and with spatially varying convective heat transfer on one face. Section 2.1 presents the general solution first. Special cases of relevance to heat transfer in semiconductor chip packaging are presented in Section 2.2.

2.1. General, M-layer case with internal heat generation

Consider thermal conduction in an M-layer rectangular slab with spatially varying heat flux $Q(x)$ on the bottom edge and spatially varying heat convective coefficient $h(x)$ on the top edge, as shown in Fig. 1. The thickness and thermal conductivity of each layer are (z_{i+1}-z_i) and k_i, respectively. Uniform heat generation q_i occurs in each layer. Further, an inter-layer thermal contact resistance R_i exists between the $(i\text{-}1)^{th}$ and i^{th} layers. Each layer is assumed to be adiabatic at the two ends in the x direction. In a rectangular coordinate system, the governing steady state energy conservation equation for T_i, the temperature rise above ambient in the i^{th} layer is expressed as:

$$k_i\frac{\partial^2 T_i}{\partial x^2}+k_i\frac{\partial^2 T_i}{\partial z^2}+q_i=0\cdot(i=1,2,3,\ldots,M) \tag{1}$$

Boundary conditions for this problem are

$$\frac{\partial T_i}{\partial x}=0\ at\ x=0,a \tag{2a}$$

$$-k_1\frac{\partial T_1}{\partial z}=Q(x)at\ z=0 \tag{2b}$$

$$-k_M\frac{\partial T_M}{\partial z}=h(x)T_M\ at\ z=z_{M+1} \tag{2c}$$

Interfacial boundary conditions accounting for temperature and heat flux continuity are

$$T_{i-1}(x,z) = T_i(x,z) - k_i R_i \frac{\partial T_i}{\partial z} \text{ at } z = z_i \tag{2d}$$

$$k_{i-1}\frac{\partial T_{i-1}}{\partial z} = k_i \frac{\partial T_i}{\partial z} \text{ at } z = z_i \cdot (i = 2,3,\ldots,M) \tag{2e}$$

The overall mathematical procedure for deriving the solution of this problem comprises of homogenization of the problem by including a term to account for internal heat generation, followed by writing an eigenfunction-based series solution. The coefficients of this series solution, which are usually given by an explicit expression in the simpler case of uniform heat transfer coefficient, are then obtained in the form of the solution of a set of linear algebraic equations involving the spatially-varying heat transfer coefficient.

In order to derive a solution for the steady-state temperature distribution in each layer, Eq. (1) is first homogenized by the following substitution:

$$T_i(x,z) = \theta_i(x,z) - \frac{q_i}{2k_i}z^2 \tag{3}$$

By substituting Eq. (3) into Eqs. (1)–(2e), the following equations are derived for $\theta_i(x,z)$:

$$\frac{\partial^2 \theta_i}{\partial x^2} + \frac{\partial^2 \theta_i}{\partial z^2} = 0 \tag{4}$$

subject to

$$\frac{\partial \theta_i}{\partial x} = 0 \text{ at } x = 0, a \tag{5a}$$

$$-k_1 \frac{\partial \theta_1}{\partial z} = Q(x) \text{ at } z = 0 \tag{5b}$$

$$k_M \frac{\partial \theta_M}{\partial z} + h(x)\theta_M = F(x) \text{ at } z = z_{M+1} \tag{5c}$$

$$\theta_{i-1}(x,z) = \theta_i(x,z) - k_i R_i \frac{\partial \theta_i}{\partial z} + z_i\left(\frac{q_{i-1}}{2k_{i-1}}z_i - \frac{q_i}{2k_i}z_i + R_i q_i\right) \text{ at } z = z_i \tag{5d}$$

$$k_{i-1}\frac{\partial \theta_{i-1}}{\partial z} + z_i(q_i - q_{i-1}) = k_i \frac{\partial \theta_i}{\partial z} \text{ at } z = z_i \tag{5e}$$

where

$$F(x) = q_M z_{M+1}\left[1 + \frac{z_{M+1}h(x)}{2k_M}\right] \tag{6}$$

In order to proceed, the heat flux $Q(x)$ is written in the form of a Fourier series

$$Q(x) = P_0 + \sum_{n=1}^{\infty} P_n \cos\left(\frac{n\pi x}{a}\right) \tag{7}$$

where

$$P_0 = \frac{1}{a}\int_0^a Q(x)dx \tag{8a}$$

$$P_n = \frac{2}{a}\int_0^a Q(x)\cos\left(\frac{n\pi x}{a}\right)dx \text{ for } n = 1,2\ldots \tag{8b}$$

Note that cosine eigenfunctions are chosen for the Fourier series expansion in order to match the required boundary conditions for the temperature distribution.

Accordingly, the solution for $\theta_i(x,z)$ may be expressed in the form of the following Fourier cosine series

$$\theta_i(x,z) = C_{i,0}(z) + \sum_{n=1}^{\infty} C_{i,n}(z)\cos\left(\frac{n\pi x}{a}\right) \tag{9}$$

Since Eq. (9) already satisfies Eq. (5a), the coefficients $C_{i,0}(z)$ and $C_{i,n}(z)$ must be determined in order to satisfy the governing Eq. (4) and boundary conditions given by Eqs. (5b)–(5e).

Using the expression for $\theta_i(x,z)$ given by Eq. (9) into Eq. (4) results in

$$C''_{i,0}(z) + \sum_{n=1}^{\infty} C''_{i,n}(z)\cos\left(\frac{n\pi x}{a}\right) - \left(\frac{n\pi}{a}\right)^2 \sum_{n=1}^{\infty} C_{i,n}(z)\cos\left(\frac{n\pi x}{a}\right) = 0 \tag{10}$$

Separately examining $C_{i,0}$ and $C_{i,n}$ results in the following expressions

$$C_{i,0}(z) = A_{i,0} + B_{i,0}z \tag{11a}$$

$$C_{i,n}(z) = A_{i,n}\exp\left(\frac{n\pi z}{a}\right) + B_{i,n}\exp\left(-\frac{n\pi z}{a}\right) \tag{11b}$$

where $A_{i,0}$, $B_{i,0}$, $A_{i,n}$ and $B_{i,n}$ are unknown coefficients for each layer i = 1,2, …,M and for each eigenvalue n = 1,2,3 …. These unknown coefficients are determined by requiring the expression for $\theta_i(x,z)$ given by Eq. (9) to satisfy the boundary conditions given by Eqs. (5b)–(5e).

By substituting Eq. (9) into Eq. (5b), and using Eqs. (7), (11a) and (11b), one may obtain

$$B_{1,0} = -\frac{P_o}{k_1} \tag{12a}$$

$$B_{1,n} = A_{1,n} + \frac{P_n a}{n\pi k_1} \tag{12b}$$

Next, by substituting Eq. (9) into Eqs. (5d) and (5e) and , and using Eqs (11a) and (11b), one may obtain

$$A_{i,0} = A_{1,0} + P_o\sum_{j=2}^{i} z_j\left(\frac{1}{k_j} - \frac{1}{k_{j-1}}\right) - \sum_{j=3}^{i} z_j\left(\frac{1}{k_j} - \frac{1}{k_{j-1}}\right)\sum_{k=2}^{j-1} z_k(q_k - q_{k-1}) - P_o\sum_{j=2}^{i} R_j - \sum_{j=2}^{i}\frac{z_j^2}{k_j}(q_j - q_{j-1}) + \sum_{j=2}^{i} R_j\sum_{k=2}^{j} z_k(q_k - q_{k-1}) + \sum_{j=2}^{i}\frac{z_j^2}{2}\left(\frac{q_j}{k_j} - \frac{q_{j-1}}{k_{j-1}}\right) - \sum_{j=2}^{i} R_j q_j z_j \tag{13a}$$

$$B_{i,0} = -\frac{P_o}{k_i} + \frac{1}{k_i}\sum_{j=2}^{i} z_j(q_j - q_{j-1}) \tag{13b}$$

Further, $A_{i,n}$ and $B_{i,n}$ can be expressed as

$$A_{i,n} = \frac{1}{2}\left[1 + (1+\phi_i)\frac{k_{i-1}}{k_i}\right]A_{i-1,n} + \frac{1}{2}\left[1 - (1+\phi_i)\frac{k_{i-1}}{k_i}\right]B_{i-1,n}\exp\left(-\frac{2n\pi z_i}{a}\right) \tag{14a}$$

$$B_{i,n} = \frac{1}{2}\left[1 + (1-\phi_i)\frac{k_{i-1}}{k_i}\right]B_{i-1,n} + \frac{1}{2}\left[1 - (1-\phi_i)\frac{k_{i-1}}{k_i}\right]A_{i-1,n}\exp\left(\frac{2n\pi z_i}{a}\right) \tag{14b}$$

The two equations above can be further simplified to write $A_{i,n}$ and $B_{i,n}$ in terms of $A_{1,n}$ as follows

$$A_{i,n} = \eta_{i,A}A_{1,n} + \mu_{i,A} \tag{15a}$$

$$B_{i,n} = \eta_{i,B}A_{1,n} + \mu_{i,B} \tag{15b}$$

where the coefficients are given by the following coupled, recursive relationships:

$$\eta_{i,A} = \frac{1}{2}\left[1 - (1+\phi_i)\frac{k_{i-1}}{k_i}\right]\eta_{i-1,B}\exp\left(-\frac{2n\pi z_i}{a}\right) + \frac{1}{2}\left[1 + (1+\phi_i)\frac{k_{i-1}}{k_i}\right]\eta_{i-1,A} \tag{16a}$$

$$\mu_{i,A} = \frac{1}{2}\left[1 - (1+\phi_i)\frac{k_{i-1}}{k_i}\right]\mu_{i-1,B}\exp\left(-\frac{2n\pi z_i}{a}\right) + \frac{1}{2}\left[1 + (1+\phi_i)\frac{k_{i-1}}{k_i}\right]\mu_{i-1,A} \tag{16b}$$

$$\eta_{i,B}=\frac{1}{2}\left[1-(1-\phi_i)\frac{k_{i-1}}{k_i}\right]\eta_{i-1,A}\exp\left(\frac{2n\pi z_i}{a}\right)+\frac{1}{2}\left[1+(1-\phi_i)\frac{k_{i-1}}{k_i}\right]\eta_{i-1,B} \tag{16c}$$

$$\mu_{i,B}=\frac{1}{2}\left[1-(1-\phi_i)\frac{k_{i-1}}{k_i}\right]\mu_{i-1,A}\exp\left(\frac{2n\pi z_i}{a}\right)+\frac{1}{2}\left[1+(1-\phi_i)\frac{k_{i-1}}{k_i}\right]\mu_{i-1,B} \tag{16d}$$

where,

$$\phi_i=\frac{n\pi k_i R_i}{a} \tag{17}$$

Initial values for these recursive relationships are given by $\eta_{1,A}=1$, $\mu_{1,A}=0$, $\eta_{1,B}=1$, $\mu_{1,B}=\frac{P_0 a}{n\pi k_1}$.

The coefficients for the M^{th} layer are of particular interest. Setting $i=M$ in Eqs. (13a), (13b), (15a) and (15b) yields

$$A_{M,0}=A_{1,0}+P_o\sum_{j=2}^{M}z_j\left(\frac{1}{k_j}-\frac{1}{k_{j-1}}\right)+f_1-g \tag{18a}$$

$$B_{M,0}=-\frac{P_o}{k_M}+f_2 \tag{18b}$$

$$A_{M,n}=\eta_{M,A}A_{1,n}+\mu_{M,A} \tag{19a}$$

$$B_{M,n}=\eta_{M,B}A_{1,n}+\mu_{M,B} \tag{19b}$$

where

$$f_1=-\sum_{j=3}^{M}z_j\left(\frac{1}{k_j}-\frac{1}{k_{j-1}}\right)\sum_{k=2}^{j-1}z_k(q_k-q_{k-1})-\sum_{j=2}^{M}\frac{z_j^2}{k_j}(q_j-q_{j-1})+\sum_{j=2}^{M}R_j\sum_{k=2}^{j}z_k(q_k-q_{k-1})+\sum_{j=2}^{M}\frac{z_j^2}{2}\left(\frac{q_j}{k_j}-\frac{q_{j-1}}{k_{j-1}}\right)-\sum_{j=2}^{M}R_jq_jz_j \tag{20a}$$

$$f_2=\frac{1}{k_M}\sum_{j=2}^{M}z_j(q_j-q_{j-1}) \tag{20b}$$

$$g=P_o\sum_{j=2}^{M}R_j \tag{21}$$

Eqs. (12a)–(15b) express all the coefficients needed to define the temperature solution – $A_{i,0}$, $B_{i,0}$, $A_{i,n}$ and $B_{i,n}$ – in terms of $A_{1,0}$ and $A_{1,n}$, $n=1,2,3\ldots$.

In order to determine $A_{1,0}$ and $A_{1,n}$, and thus complete the solution, Eq. (9) is substituted into the boundary condition involving spatially varying heat transfer coefficient, Eq. (5c). Using Eqs. (11a) and (11b), with $i=M$ as well as Eqs. (18a)–(19b), one obtains an expression involving the spatially varying heat transfer coefficient $h(x)$

$$A_{1,0}h(x)+P_0\sum_{j=2}^{M}z_j\left(\frac{1}{k_j}-\frac{1}{k_{j-1}}\right)h(x)+f_1h(x)-gh(x)-F(x)+z_{M+1}f_2h(x)+f_2k_M+\sum_{n=1}^{\infty}\left(\eta_{M,A}A_{1,n}+\mu_{M,A}\right)\exp\left(\frac{n\pi z_{M+1}}{a}\right)\cos\left(\frac{n\pi x}{a}\right)h(x)+\sum_{n=1}^{\infty}\frac{n\pi k_M}{a}\left(\eta_{M,A}A_{1,n}+\mu_{M,A}\right)\exp\left(\frac{n\pi z_{M+1}}{a}\right)\cos\left(\frac{n\pi x}{a}\right)=P_0\left(1+\frac{z_{M+1}h(x)}{k_M}\right)+\sum_{n=1}^{\infty}\left(\eta_{M,B}A_{1,n}+\mu_{M,B}\right)\exp\left(-\frac{n\pi z_{M+1}}{a}\right)\cos\left(\frac{n\pi x}{a}\right)\left(\frac{n\pi k_M}{a}-h(x)\right) \tag{22}$$

Eq. (22) involves the unknown coefficients $A_{1,0}$ and $A_{1,n}$ that must be determined. For the case of uniform h, this is usually carried out using the principle of orthogonality, wherein all terms except one drop out. In this more general case, a set of linear equations in the unknown coefficients is derived. While the summations in Eq. (22) involve, in principle, an infinite number of eigenvalues, a total of N terms is considered in the summations in Eq. (22). Integrating Eq. (22) from $x=0$ to $x=a$, one may obtain a linear algebraic equation as follows

$$A_{1,0}\int_0^a h(x)dx+P_0\sum_{j=2}^{M}z_j\left(\frac{1}{k_j}-\frac{1}{k_{j-1}}\right)\int_0^a h(x)dx+f_1\int_0^a h(x)dx-g\int_0^a h(x)dx-\int_0^a F(x)dx+z_{M+1}f_2\int_0^a h(x)dx+f_2k_Ma+\sum_{n=1}^{N}\left(\eta_{M,A}A_{1,n}+\mu_{M,A}\right)\exp\left(\frac{n\pi z_{M+1}}{a}\right)\int_0^a h(x)\cos\left(\frac{n\pi x}{a}\right)dx=P_0a+\frac{P_0z_{M+1}}{k_M}\int_0^a h(x)dx-\sum_{n=1}^{N}\left(\eta_{M,B}A_{1,n}+\mu_{M,B}\right)\exp\left(-\frac{n\pi z_{M+1}}{a}\right)\int_0^a h(x)\cos\left(\frac{n\pi x}{a}\right)dx \tag{23}$$

Also, multiplying both sides of equation (22) by $\cos\left(\frac{i\pi x}{a}\right)$ for $i=1,2,\ldots,N$ and then integrating from $x=0$ to $x=a$ results in

$$A_{1,0}\int_0^a h(x)\cos\left(\frac{i\pi x}{a}\right)dx+P_0\sum_{j=2}^{M}z_j\left(\frac{1}{k_j}-\frac{1}{k_{j-1}}\right)\int_0^a h(x)\cos\left(\frac{i\pi x}{a}\right)dx+f_1\int_0^a h(x)\cos\left(\frac{i\pi x}{a}\right)dx-g\int_0^a h(x)\cos\left(\frac{i\pi x}{a}\right)dx-\int_0^a F(x)\cos\left(\frac{i\pi x}{a}\right)dx+z_{M+1}f_2\int_0^a h(x)\cos\left(\frac{i\pi x}{a}\right)dx+\sum_{n=1}^{N}\left(\eta_{M,A}A_{1,n}+\mu_{M,A}\right)\exp\left(\frac{n\pi z_{M+1}}{a}\right)\int_0^a h(x)\cos\left(\frac{n\pi x}{a}\right)\cos\left(\frac{i\pi x}{a}\right)dx+\frac{i\pi k_M}{2}\left(\eta_{M,A}A_{1,i}+\mu_{M,A}\right)\exp\left(\frac{i\pi z_{M+1}}{a}\right)=\frac{P_0z_{M+1}}{k_M}\int_0^a h(x)\cos\left(\frac{i\pi x}{a}\right)dx+\frac{i\pi k_M}{2}\left(\eta_{M,B}A_{1,i}+\mu_{M,B}\right)\exp\left(-\frac{i\pi z_{M+1}}{a}\right)-\sum_{n=1}^{N}\left(\eta_{M,B}A_{1,n}+\mu_{M,B}\right)\exp\left(-\frac{n\pi z_{M+1}}{a}\right)\int_0^a h(x)\cos\left(\frac{n\pi x}{a}\right)\cos\left(\frac{i\pi x}{a}\right)dx \tag{24}$$

Note that derivation of Eq. (24) used the orthogonality of the eigenfunctions

$$\int_0^a\cos\left(\frac{i\pi x}{a}\right)\cos\left(\frac{n\pi x}{a}\right)dx=\begin{cases}0 & i\neq n\\ \frac{a}{2} & i=n\end{cases} \tag{25}$$

Eqs. (23) and (24) represent $(N+1)$ linear algebraic equations involving $(N+1)$ unknowns, $A_{1,0}$ and $A_{1,i}$ $(i=1,2,\ldots,N)$. These equations can be easily solved using well-known methods such as matrix inversion. In the present work, matrix inversion is carried out using the LU decomposition method, which is known to be an efficient method for matrix decomposition. Once these coefficients are determined, Eq. (3), along with Eqs. (9), (11a), (11b), (12a), (12b), (13a), (13b), (15a) and (15b) represent the final solution for temperature distribution in the composite body.

2.2. Special cases

2.2.1. Zero internal heat generation

The case of zero internal heat generation is of interest in semiconductor packaging problems where heat from the semiconductor chip enters the multi-layer packaging, but there is no internal heat generation in the packaging itself. In case there is no internal heat generation in the multi-layer body, i.e., $q_i=0$, Eq. (1) is directly converted to Eq. (4) with boundary conditions (2a)-(2e). Accordingly, all the terms related to

internal heat generations in Eqs. (13a) and (13b) are equal to zero, namely

$$A_{i,0} = A_{1,0} + P_o \sum_{j=2}^{i} z_j \left(\frac{1}{k_j} - \frac{1}{k_{j-1}}\right) - P_o \sum_{j=2}^{i} R_j \tag{26a}$$

$$B_{i,0} = -\frac{P_o}{k_i} \tag{26b}$$

Further, $F(x)$, f_1 and f_2 in Eqs. (5c), (18a) and (18b) are all zero. This results in simplification of Eq. (23) and (24) as follows

$$\begin{aligned} &A_{1,0}\int_0^a h(x)dx + P_0 \sum_{j=2}^{M} z_j \left(\frac{1}{k_j} - \frac{1}{k_{j-1}}\right) \int_0^a h(x)dx - g\int_0^a h(x)dx \\ &+ \sum_{n=1}^{N} \left(\eta_{M,A} A_{1,n} + \mu_{M,A}\right) \exp\left(\frac{n\pi z_{M+1}}{a}\right) \int_0^a h(x)\cos\left(\frac{n\pi x}{a}\right)dx \\ &= P_0 a + \frac{P_0 z_{M+1}}{k_M} \int_0^a h(x)dx - \sum_{n=1}^{N} \left(\eta_{M,B} A_{1,n} + \mu_{M,B}\right) \\ &\exp\left(-\frac{n\pi z_{M+1}}{a}\right) \int_0^a h(x)\cos\left(\frac{n\pi x}{a}\right)dx \end{aligned} \tag{27}$$

and

$$\begin{aligned} &A_{1,0}\int_0^a h(x)\cos\left(\frac{i\pi x}{a}\right)dx + P_0 \sum_{j=2}^{M} z_j \left(\frac{1}{k_j} - \frac{1}{k_{j-1}}\right) \int_0^a h(x)\cos\left(\frac{i\pi x}{a}\right)dx - \\ &g\int_0^a h(x)\cos\left(\frac{i\pi x}{a}\right)dx + \sum_{n=1}^{N} \left(\eta_{M,A} A_{1,n} + \mu_{M,A}\right) \exp\left(\frac{n\pi z_{M+1}}{a}\right) \\ &\int_0^a h(x)\cos\left(\frac{n\pi x}{a}\right)\cos\left(\frac{i\pi x}{a}\right)dx + \frac{i\pi k_M}{2} \left(\eta_{M,A} A_{1,i} + \mu_{M,A}\right)\exp\left(\frac{i\pi z_{M+1}}{a}\right) \\ &= \frac{P_0 z_{M+1}}{k_M} \int_0^a h(x)\cos\left(\frac{i\pi x}{a}\right)dx + \frac{i\pi k_M}{2} \left(\eta_{M,B} A_{1,i} + \mu_{M,B}\right)\exp\left(-\frac{i\pi z_{M+1}}{a}\right) \\ &- \sum_{n=1}^{N} \left(\eta_{M,B} A_{1,n} + \mu_{M,B}\right) \exp\left(-\frac{n\pi z_{M+1}}{a}\right) \int_0^a h(x)\cos\left(\frac{n\pi x}{a}\right)\cos\left(\frac{i\pi x}{a}\right)dx \end{aligned} \tag{28}$$

Similar to the general case, Eqs. (27) and (28) represent a set of $(N+1)$ linear equations in unknowns $A_{1,0}$ and $A_{1,i}$ $(i = 1,2, \ldots,N)$ that can be easily solved using matrix inversion to determine the temperature distribution for this special case.

2.2.2. Zero thermal contact resistance

Perfect thermal contact between adjacent layers is also a relevant assumption in several applications. In such a case, the boundary condition (2d) is given by

$$T_{i-1}(x,z) = T_i(x,z) \text{ at } z = z_i \tag{29}$$

Accordingly, $g = 0$ in Eq. (18a), and, therefore, Eq. (18a) further reduces to

$$A_{M,0} = A_{1,0} + P_o \sum_{j=2}^{M} z_j \left(\frac{1}{k_j} - \frac{1}{k_{j-1}}\right) + f_1 \tag{30}$$

Eq. (17) shows that, in this case, $\phi_i = 0$. Therefore, Eqs. (16a)-(16d) are simplified as

$$\eta_{i,A} = \frac{1}{2}\left[1 - \frac{k_{i-1}}{k_i}\right]\eta_{i-1,B} \exp\left(-\frac{2n\pi z_i}{a}\right) + \frac{1}{2}\left[1 + \frac{k_{i-1}}{k_i}\right]\eta_{i-1,A} \tag{31a}$$

$$\mu_{i,A} = \frac{1}{2}\left[1 - \frac{k_{i-1}}{k_i}\right]\mu_{i-1,B} \exp\left(-\frac{2n\pi z_i}{a}\right) + \frac{1}{2}\left[1 + \frac{k_{i-1}}{k_i}\right]\mu_{i-1,A} \tag{31b}$$

$$\eta_{i,B} = \frac{1}{2}\left[1 - \frac{k_{i-1}}{k_i}\right]\eta_{i-1,A} \exp\left(\frac{2n\pi z_i}{a}\right) + \frac{1}{2}\left[1 + \frac{k_{i-1}}{k_i}\right]\eta_{i-1,B} \tag{31c}$$

$$\mu_{i,B} = \frac{1}{2}\left[1 - \frac{k_{i-1}}{k_i}\right]\mu_{i-1,A} \exp\left(\frac{2n\pi z_i}{a}\right) + \frac{1}{2}\left[1 + \frac{k_{i-1}}{k_i}\right]\mu_{i-1,B} \tag{31d}$$

Finally, the set of linear algebraic equations solving unknowns $A_{1,0}$ and $A_{1,\,i}$ $(i = 1,2, \ldots,N)$ is given by

$$\begin{aligned} &A_{1,0}\int_0^a h(x)dx + P_0 \sum_{j=2}^{M} z_j \left(\frac{1}{k_j} - \frac{1}{k_{j-1}}\right) \int_0^a h(x)dx + f_1 \int_0^a h(x)dx - \int_0^a F(x)dx \\ &+ z_{M+1} f_2 \int_0^a h(x)dx + f_2 k_M a + \sum_{n=1}^{N} \left(\eta_{M,A} A_{1,n} + \mu_{M,A}\right) \exp\left(\frac{n\pi z_{M+1}}{a}\right) \\ &\int_0^a h(x)\cos\left(\frac{n\pi x}{a}\right)dx = P_0 a + \frac{P_0 z_{M+1}}{k_M} \int_0^a h(x)dx - \sum_{n=1}^{N} \left(\eta_{M,B} A_{1,n} + \mu_{M,B}\right) \\ &\exp\left(-\frac{n\pi z_{M+1}}{a}\right) \int_0^a h(x)\cos\left(\frac{n\pi x}{a}\right)dx \end{aligned} \tag{32}$$

and

$$\begin{aligned} &A_{1,0}\int_0^a h(x)\cos\left(\frac{i\pi x}{a}\right)dx + P_0 \sum_{j=2}^{M} z_j \left(\frac{1}{k_j} - \frac{1}{k_{j-1}}\right) \int_0^a h(x)\cos\left(\frac{i\pi x}{a}\right)dx \\ &+ f_1 \int_0^a h(x)\cos\left(\frac{i\pi x}{a}\right)dx - \int_0^a F(x)\cos\left(\frac{i\pi x}{a}\right)dx \\ &+ z_{M+1} f_2 \int_0^a h(x)\cos\left(\frac{i\pi x}{a}\right)dx + \sum_{n=1}^{N} \left(\eta_{M,A} A_{1,n} + \mu_{M,A}\right) \\ &\exp\left(\frac{n\pi z_{M+1}}{a}\right) \int_0^a h(x)\cos\left(\frac{n\pi x}{a}\right)\cos\left(\frac{i\pi x}{a}\right)dx + \frac{i\pi k_M}{2} \left(\eta_{M,A} A_{1,i} + \mu_{M,A}\right) \\ &\exp\left(\frac{i\pi z_{M+1}}{a}\right) = \frac{P_0 z_{M+1}}{k_M} \int_0^a h(x)\cos\left(\frac{i\pi x}{a}\right)dx + \frac{i\pi k_M}{2} \left(\eta_{M,B} A_{1,i} + \mu_{M,B}\right) \\ &\exp\left(-\frac{i\pi z_{M+1}}{a}\right) - \sum_{n=1}^{N} \left(\eta_{M,B} A_{1,n} + \mu_{M,B}\right) \exp\left(-\frac{n\pi z_{M+1}}{a}\right) \\ &\int_0^a h(x)\cos\left(\frac{n\pi x}{a}\right)\cos\left(\frac{i\pi x}{a}\right)dx \end{aligned} \tag{33}$$

2.2.3. Two-layer body with zero internal heat generation

This sub-section considers a simplified case of a two-layer body with no internal heat generation. This could model, for example, a chip-package stack with a non-zero thermal contact resistance between the two. In such a case, Eq. (26a) directly reduces to

$$A_{2,0} = A_{1,0} + P_o z_2 \left(\frac{1}{k_2} - \frac{1}{k_1}\right) - P_o R_2 \tag{34}$$

Accordingly, Eqs. (27) and (28) simplify to

$$\begin{aligned} &A_{1,0}\int_0^a h(x)dx + P_0 z_2 \left(\frac{1}{k_2} - \frac{1}{k_1}\right) \int_0^a h(x)dx - P_o R_2 \int_0^a h(x)dx \\ &+ \sum_{n=1}^{N} \left(\eta_{2,A} A_{1,n} + \mu_{2,A}\right) \exp\left(\frac{n\pi z_3}{a}\right) \int_0^a h(x)\cos\left(\frac{n\pi x}{a}\right)dx \\ &= P_0 a + \frac{P_0 z_3}{k_2} \int_0^a h(x)dx - \sum_{n=1}^{N} \left(\eta_{2,B} A_{1,n} + \mu_{2,B}\right) \exp\left(-\frac{n\pi z_3}{a}\right) \int_0^a h(x)\cos\left(\frac{n\pi x}{a}\right)dx \end{aligned} \tag{35}$$

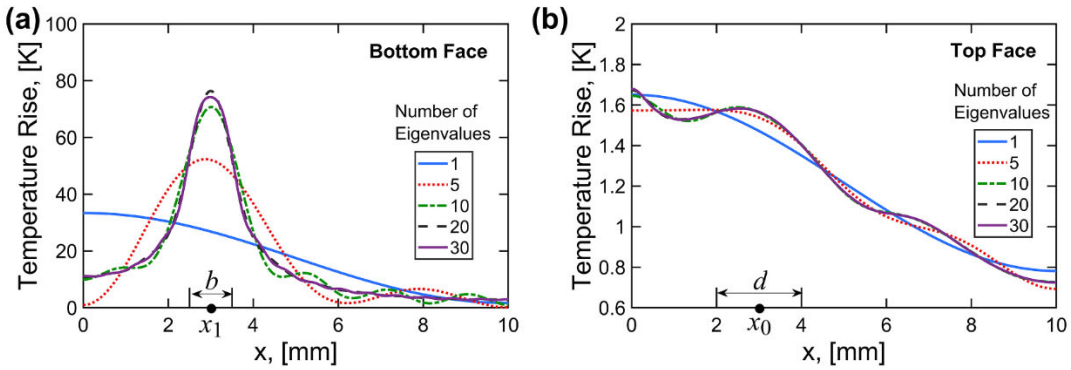

Fig. 2. Effect of number of eigenvalues considered: (a) and (b) plot temperature distribution along the bottom and top faces, respectively, for 1, 5, 10, 20 and 30 eigenvalues. This figure considers a three-layer geometry with step heating on the bottom face and convective heat transfer coefficient representative of jet impingement cooling at the top face.

and

$$A_{1,0}\int_0^a h(x)\cos\left(\frac{i\pi x}{a}\right)dx + P_0 z_2\left(\frac{1}{k_2}-\frac{1}{k_1}\right)\int_0^a h(x)\cos\left(\frac{i\pi x}{a}\right)dx - P_o R_2$$
$$\int_0^a h(x)\cos\left(\frac{i\pi x}{a}\right)dx + \sum_{n=1}^{N}\left(\eta_{2,A}A_{1,n}+\mu_{2,A}\right)\exp\left(\frac{n\pi z_3}{a}\right)$$
$$\int_0^a h(x)\cos\left(\frac{n\pi x}{a}\right)\cos\left(\frac{i\pi x}{a}\right)dx + \frac{i\pi k_2}{2}\left(\eta_{2,A}A_{1,i}+\mu_{2,A}\right)\exp\left(\frac{i\pi z_3}{a}\right)$$
$$= \frac{P_0 z_3}{k_2}\int_0^a h(x)\cos\left(\frac{i\pi x}{a}\right)dx + \frac{i\pi k_2}{2}\left(\eta_{2,B}A_{1,i}+\mu_{2,B}\right)\exp\left(-\frac{i\pi z_3}{a}\right)$$
$$-\sum_{n=1}^{N}\left(\eta_{2,B}A_{1,n}+\mu_{2,B}\right)\exp\left(-\frac{n\pi z_3}{a}\right)\int_0^a h(x)\cos\left(\frac{n\pi x}{a}\right)\cos\left(\frac{i\pi x}{a}\right)dx \tag{36}$$

The linear algebraic Eqs. (35) and (36) can be solved using matrix inversion to determine the solution for this special case. Note that for this two-layer problem, the four coefficients $\eta_{2,A}$, $\mu_{2,A}$, $\eta_{2,B}$ and $\mu_{2,B}$ are given by

$$\eta_{2,A} = \frac{1}{2}\left[1-(1+\phi_2)\frac{k_1}{k_2}\right]\exp\left(-\frac{2n\pi z_2}{a}\right) + \frac{1}{2}\left[1+(1+\phi_2)\frac{k_1}{k_2}\right] \tag{37a}$$

$$\mu_{2,A} = \frac{1}{2}\left[1-(1+\phi_2)\frac{k_1}{k_2}\right]\frac{P_n a}{n\pi k_1}\exp\left(-\frac{2n\pi z_2}{a}\right) \tag{37b}$$

$$\eta_{2,B} = \frac{1}{2}\left[1-(1-\phi_2)\frac{k_1}{k_2}\right]\exp\left(\frac{2n\pi z_2}{a}\right) + \frac{1}{2}\left[1+(1-\phi_2)\frac{k_1}{k_2}\right] \tag{37c}$$

$$\mu_{2,B} = \frac{1}{2}\left[1+(1-\phi_2)\frac{k_1}{k_2}\right]\frac{P_n a}{n\pi k_1} \tag{37d}$$

3. Results and discussion

This section discusses key results obtained from the analytical solution presented in Section 2. Verification of the solution is discussed first. This is followed by discussion of the application of the solution for a number of multilayer problems. In each case, spatially dependent convective heat transfer is assumed on one face of the multilayer body. An expression for $h(x)$ representative of convective heat transfer due to impingement cooling by a slot jet [24] is used as follows:

$$h(x) = h_{max}\left[\frac{1-R\tanh\left(\gamma\left(\frac{|x-x_0|}{d}-1.5\right)\right)}{1+R}\right] \tag{38}$$

where x_0 and d refer to the location of the centerline of the jet and jet width, respectively. Further, $R = \frac{h_{max}-h_{min}}{h_{max}+h_{min}}$. In this definition, $h_{\max}$ and $h_{\min}$ stand for the convective heat transfer coefficients in the jet slot and far away from the jet, separately. The parameter γ is representative of how sharply the h vs x curve transitions between $h_{\min}$ and $h_{\max}$. This equation models convective heat transfer due to an impinging jet – both circular and slot – which is highest at the site of impingement and reduces sharply outwards.

3.1. Verification and effect of number of eigenvalues

As is the case with eigenvalue-based solutions of thermal conduction problems, the accuracy of results derived here depends strongly on the number of eigenvalues considered in the solution. In this specific case, the number of eigenvalues also determines the size of the matrix that must be inverted in order to calculate the unknown coefficients $A_{1,0}$ and

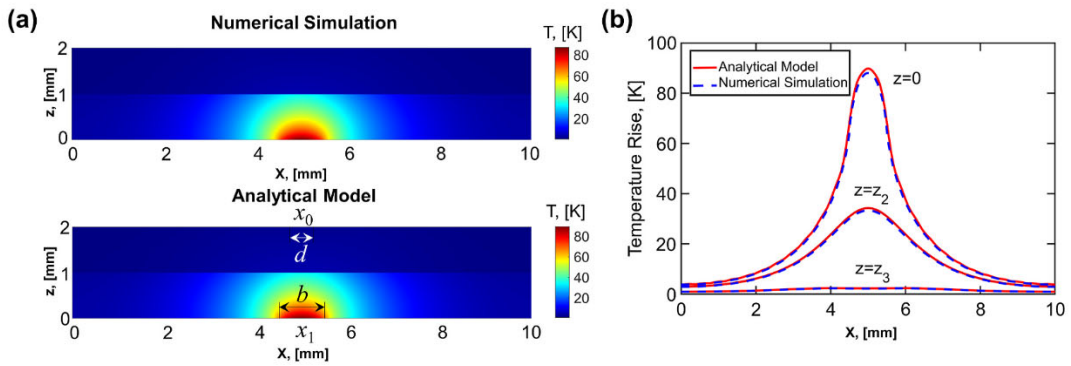

Fig. 3. Validation of the analytical solution by comparison with finite-element simulation results for a two-layer body: (a) compares colorplots of temperature distribution computed by the analytical solution and predicted by the numerical simulation; (b) compares temperature distribution at three z locations.

$A_{1,n}$. In order to determine the minimum number of eigenvalues needed for an accurate solution with acceptable computational cost, the impact of number of eigenvalues on temperature distribution is investigated for a representative three-layer problem with step-function heating at the bottom face and a spatially-varying convective heat transfer coefficient representative of jet impingement cooling, as given by Eq. (38), on the top face. For this representative problem, the magnitude, width and center of the step-function heat flux is taken to be 1.1×10^5 W/m^2, $b = 1$ mm and $x_1 = 3.0$ mm, respectively. Jet impingement cooling centered at $x_0 = 3.0$ mm on the top face is assumed, with $h_{\min} = 5000$ W/m^{2}K, $h_{\max} = 10{,}000$ W/m^{2}K, $d = 2.0$ mm and $\gamma = 2.0$. Thermal conductivities of the layers are 1, 10 and 2 W/mK, respectively. Internal heat generation rates of 10,000 W/m^3 are considered in each layer of thickness 1 mm. In addition, a thermal contact resistance of 10^{-5} Km^2/W is assumed between adjacent layers. For these parameters, Fig. 2(a) and (b) and plot the bottom face and top face temperature distributions for different number of eigenvalues. These plots show some periodicity characteristic with representing a function with a periodic Fourier series. Both plots show that as the number of eigenvalues increases, the computed temperature distribution changes, and stabilizes around 20–30 eigenvalues. There is minimal change in the computed temperature distribution between 20 and 30 eigenvalues. This helps establish the minimum number of eigenvalues needed for reliable computation for the parameter values considered here. All further computations in this paper are carried out with 30 eigenvalues. Note that this is not a particularly large number of eigenvalues, since the series solutions for such problems are known to converge algebraically [26]. Even with 30 eigenvalues, the computational time on a standard desktop computer is found to be minimal. Specifically, the matrices generated from Eqs. (23) and (24) can be inverted in less than 0.3 s in standard scientific computation software. It is possible, however, that for other problems that may require more number of eigenvalues, the computational burden for matrix inversion can be significant, in which case, computational optimization of the matrix inversion process may be needed.

Fig. 3 presents results from comparison of the analytical solution with finite-element simulations. For this comparison, a two-layer body with step function heat flux at the bottom and jet impingement cooling at the top is considered. Thermal conductivities of the two layers are 1 and 10 W/mK, respectively, while the thicknesses are both 1 mm. Heat generation rates in the two layers are 5×10^4 and 10^4 W/m^3, respectively. Thermal contact resistance of 10^{-3} Km^2/W is considered. A step-function heat flux on the bottom face has magnitude of 10^5 W/m^2, width of $b = 1$ mm and is centered at $x_1 = 5$ mm. Jet impingement cooling is assumed with a jet centered at $x_0 = 5.0$ mm on the top face. The spatially varying convective heat transfer coefficient for each jet is given by Eq. (38), with $h_{\min} = 10^4$ W/m^{2}K, $h_{\max} = 5000$ W/m^{2}K, $d = 0.5$ mm and $\gamma = 2.0$.

For these parameters, the temperature distribution is computed using the analytical solution presented in Section 2. For comparison, finite-element simulations are carried out in ANSYS-CFX. A geometric model of a two-layer body similar to the one used in the analytical solution is created and meshed. After carrying out a mesh sensitivity study, the total number of 200 K elements is used, since further mesh refinement is not found to alter the results significantly. Spatially varying heat flux at the bottom surface as well as convection with space-dependent heat transfer coefficient at the top surface is implemented in the numerical solver. Solver controls are adjusted to run the simulation either for 1000 iterations or until the residual reaches 10^{-8}. Fig. 3(a) compares the complete two-dimensional temperature distribution as a function of x and z predicted by the analytical solution and computed numerically. There is excellent agreement between the two. As expected, most of the temperature gradient occurs in the first layer due to its lower thermal conductivity. Fig. 3(b) plots temperature distributions in x direction at three different cross-sections corresponding to the bottom face, interface and top face. In each case, there is excellent agreement between the analytical solution and finite-element simulation results.

Table 1
Values of various parameters for a 20-layer problem solved to demonstrate the capabilities of the analytical solution.

Layer #	Thickness (mm)	Thermal Conductivity (W/mK)	Heat Generation Rate (W/m^3)	Contact resistance with previous layer ($\times 10^{-5}$ Km^2/W)
1	5	4	20,000	
2	1	8	10,000	10
3	2	6	1800	15
4	1	10	15,000	20
5	0.5	15	2500	8
6	0.9	16	2000	5
7	0.3	21	1900	10
8	0.4	18	10,000	7
9	1	5	9000	9
10	0.6	7	18,000	3
11	2	6	12,000	5
12	0.4	1	11,000	4
13	1.2	8	5000	20
14	1.5	4	8000	6
15	0.1	3	2000	10
16	0.3	11	3000	8
17	1	13	9800	3
18	2	5	10,500	15
19	0.8	8	5000	6
20	3	4	10,000	9

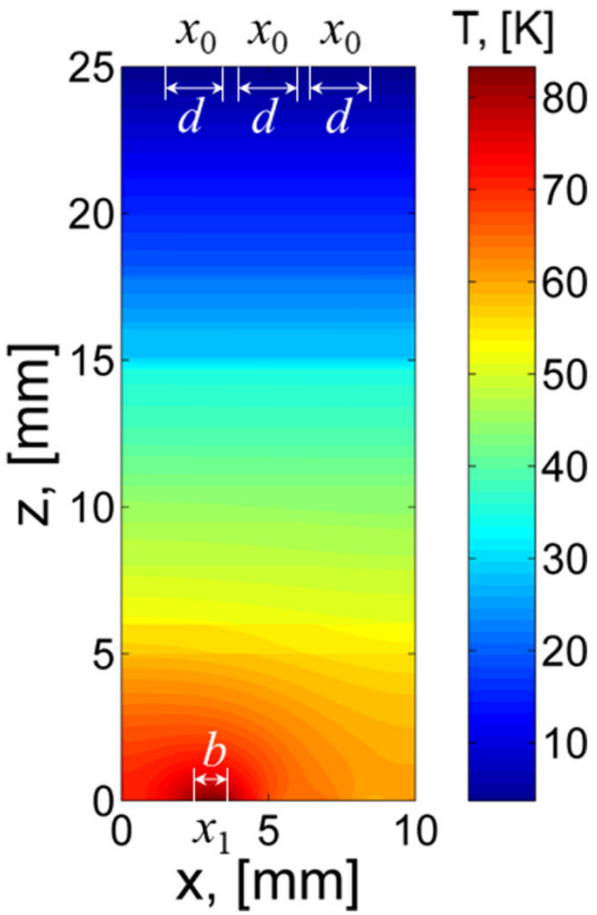

Fig. 4. Temperature colormap for the 20-layer problem defined in Section 3.2 and Table 1.

For further verification of the analytical solution presented in Section 2, temperature distribution is calculated using the solution for a special case of a two-layer body with thermal contact resistance and internal heat generation, and with constant Q and h. In such a case, the solution

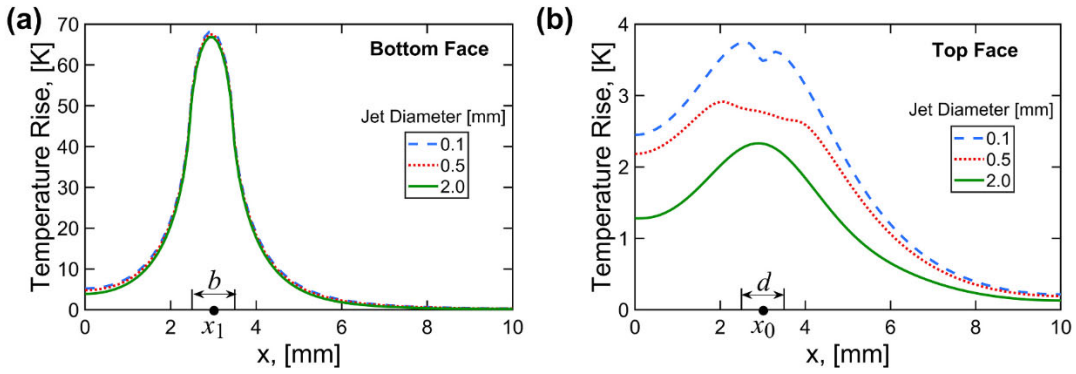

Fig. 5. Plots showing the impact of jet width on temperature distribution for a two-layer case with 1 mm wide heating of magnitude 10^5 W/m^2 on the bottom face, and jet impingement cooling given by Eq. (38) on the top face. (a) and (b) plot temperature distributions on the bottom and top faces, respectively.

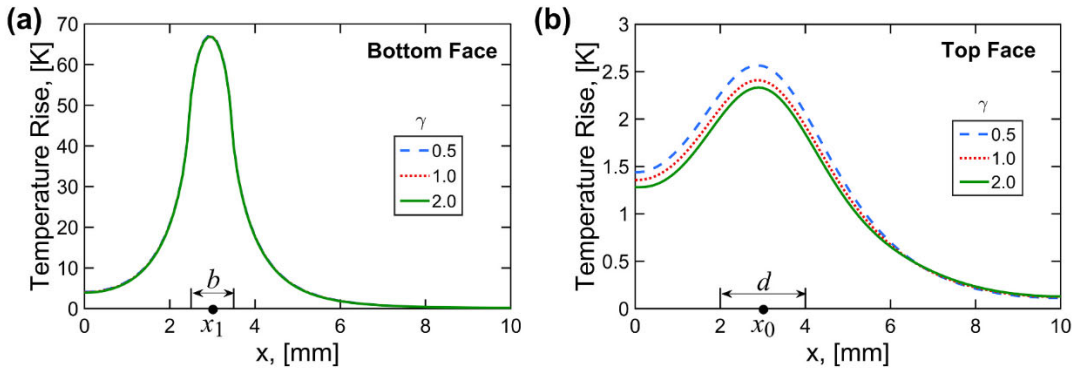

Fig. 6. Plots showing the impact of γ on temperature distribution for a two-layer case with 1 mm wide heating of magnitude 10^5 W/m^2 on the bottom face, and jet impingement cooling given by Eq. (38) on the top face. (a) and (b) plot temperature distributions on the bottom and top faces, respectively.

of the problem can be significantly simplified. Specifically, $p_0 = Q$, $p_n = 0$ for $n = 1,2,3..$, and several terms in Eqs. (23) and (24) drop out due to constant h. Further simplification results in the following temperature distribution for this special case:

$$T_1(z) = -\frac{q_1}{2k_1}z^2 - \frac{Q}{k_1}z + d_1$$
$$T_2(z) = -\frac{q_2}{2k_2}z^2 + \frac{(q_2 - q_1)z_2 - Q}{k_2}z + d_2 \tag{39}$$

where

$$d_1 = \left(\frac{q_1}{2k_1} - \frac{q_2}{2k_2}\right)z_2^2 + \left(\frac{1}{k_1} - \frac{1}{k_2}\right)Qz_2 + \frac{q_2 - q_1}{k_2}z_2^2 + R_2q_2z_2 - (q_2 - q_1)R_2z_2 + R_2Q + d_2 \tag{40}$$

$$d_2 = \frac{q_2z_3 + Q - (q_2 - q_1)z_2}{h} + \frac{q_2}{2k_2}z_3^2 - \frac{(q_2 - q_1)z_2 - Q}{k_2}z_3 \tag{41}$$

This result is identical to a straight-forward derivation of the one-dimensional temperature distribution for this problem. Therefore, for this special case, the analytical model correctly reduces to the exact

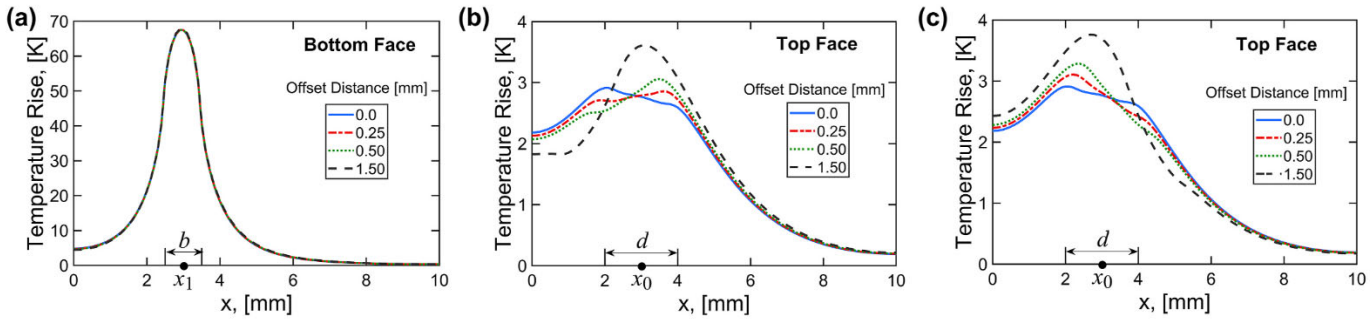

Fig. 7. Temperature distribution on the bottom face of a two-layer body for different values of the offset distance between the center of the jet and center of the hotspot. (a) Plots bottom face temperature distribution, (b) and (c) plot top face temperature distributions when the jet is offset by various distances to the left or right, respectively. The hotspot is 1 mm wide with magnitude of 10^5 W/m^2, and jet impingement cooling given by Eq. (38) on the top face. In this case, the hotspot width is 1 mm and jet diameter is 2 mm.

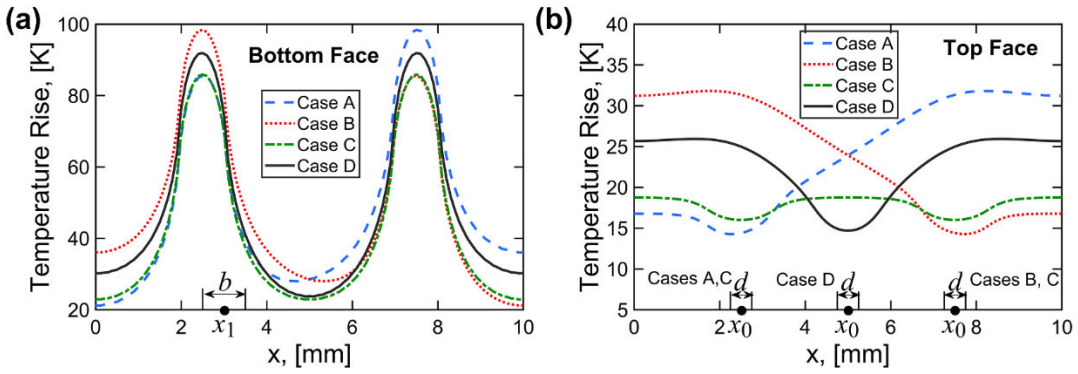

Fig. 8. Top and bottom face temperature distributions for four cases of a resource optimization problem, where a fixed total coolant flowrate is to be utilized for cooling of two hotspots. (a) and (b) plot bottom and top face temperature distributions, respectively.

solution of the problem, which provides further confidence in the analytical solution.

3.2. Results for a general, 20-layer case

In order to demonstrate the capabilities of the analytical solution for solving complicated, multi-layer problems, a 20-layer problem is formulated and solved. Table 1 summarizes the problem definition, including thicknesses, thermal conductivities and heat generation rates in each layer. Inter-layer thermal contact resistances between adjacent layers are also listed. In addition, this problem assumes step-function heat flux of magnitude 10^5 W/m^2 and 1 mm width centered at $x_1 = 3$ mm on the bottom face. Jet impingement cooling due to three separate jets centered at $x_0 = 2.5$ mm, $x_0 = 5.0$ mm and $x_0 = 7.5$ mm on the top face is assumed. The spatially varying convective heat transfer coefficient for each jet is given by Eq. (38), with $h_{\min} = 1666$ W/m^{2}K, $h_{\max} = 3333$ W/m^{2}K, $d = 2.0$ mm and $\gamma = 2.0$.

Temperature distribution for this 20-layer problem is computed using the analytical solution and presented as a colormap in Fig. 4 for the entire 20-layer body. As expected, the peak temperature occurs in the bottom-most layer, which has the highest heat generation rate and is also next to the external heat flux. The x location of the peak temperature matches well with the peak of the heat flux distribution. This Figure demonstrates the capability of the analytical solution to account for several heat generation and heat transfer phenomena, including the spatially varying convective boundary condition, in complicated multilayer problems.

3.3. Effect of h(x) parameters on temperature distribution

The impact of jet impingement cooling parameters on temperature distribution of a multi-layer stack is investigated next. The spatially varying convective heat transfer coefficient due to jet impingement is given by Eq. (38), in which, d refers to the jet diameter, and γ represents the width of the h curve. $h_{\min}$ and $h_{\max}$ are lower and upper values of the convective heat transfer coefficient, respectively. The effect of the values of these parameters on the temperature distribution is examined. In all Figures in this subsection, the thicknesses of the two layers are 1 mm each, heat generation rates are 10,000 W/m^3 each, thermal conductivities are 1 and 10 W/mK, respectively and thermal contact resistance between two layers is 10^{-5} Km^2/W, which is consistent with the reported thermal contact resistance between chips in a three-dimensional integrated circuit (3D IC) [27]. In addition, a step function heat flux with magnitude of 10^5 W/m^2, $b = 1$ mm width and centered about $x_1 = 3$ mm is applied on the bottom face.

Fig. 5(a) and (b) and plot the temperature distributions on the bottom and top faces of a two-layer body for three different values of d. Other parameters for $h(x)$ include $h_{\max} = 10{,}000$ W/m^{2}K, $h_{\min} = 5000$ W/m^{2}K and $\gamma = 2$. As expected, Fig. 5 shows that while increasing the jet width reduces the temperature distribution on the top face where the jet impinges, it has relatively little impact on the bottom, heat flux face. Note that the impact of jet width can be seen, particularly for the $d = 0.1$ mm case in the top face temperature plot.

Fig. 6 presents plots that examine the impact of the jet impingement parameter γ, which represents the sharpness/flatness of the peak region in the convective heat transfer coefficient curve. For the same problem as in Fig. 5, and with $d = 2.0$ mm, Fig. 6(a) and (b) plot temperature distributions on the bottom and top faces, respectively, for three different values of γ. Fig. 6(a) shows there is minimal impact of changing γ on temperature distribution on the bottom face. On the other hand, Fig. 6(b) shows reduction in temperature distribution near the location of jet impingement as γ increases. This is likely due to increased convection in the peak region at larger values of γ. In contrast, and as expected, the temperature distribution on the top face away from the jet location is not affected significantly by changes in γ.

Fig. 7 investigates the impact of the offset distance between the centers of the step-function heat flux on the bottom face and the jet impingement cooling on the top face. This is an important consideration in semiconductor chip cooling because of the critical need to cool multiple hotspots by strategically positioning cooling jets. In addition, it is important to understand the impact of deviations in jet locations that may occur due to manufacturing limitations. The distance between the centers of the hotspot and jet is varied for the same problem as discussed in Figs. 5 and 6, with $d = 0.5$ mm and $\gamma = 2$. Fig. 7(a) plots the bottom face temperature distribution when the jet is offset to the left by different distances. On the other hand, Fig. 7(b) and (c) and plot temperature distribution on the top face for cases where the jet is displaced to the left and right, respectively, by different offset distances. Fig. 7(a) shows that there is no discernible impact of the offset on temperature on the bottom face. On the other hand, the offset impacts temperature on the top face, as shown in Fig. 7(b) and (c). Positioning the jet at the center of the hotspot results in the least temperature rise on the top face. When the jet is moved to the left, as shown in Fig. 7(b), the impact of the jet on temperature distribution also shifts to the left, and a greater peak in temperature rise is seen. The larger the offset, the greater is the peak, which occurs away from the jet location. When the jet is shifted to the right, as shown in Fig. 7(c), the peak in temperature rise occurs towards the right. For the 1.5 mm offset case shown in Fig. 7(b) and (c), the jet is completely outside the hotspot, and the peak in temperature rise on the top face is much larger than the other cases considered.

Fig. 8 presents the investigation of a resource optimization problem for thermal management of multiple hotspots based on the analytical solution discussed in Section 2. In this problem, a two-layer body is considered, with two hotspots of equal heat flux and widths on the bottom face. Jet impingement on the top face is being used to cool the two-layer body. Since a limited amount of coolant flowrate is available for cooling the two hotspots, multiple thermal management options are possible in terms of the number and locations of the jets. The entire flowrate could be directed to either the left or right hotspot (Cases A and B, respectively). Another option is to split the flowrate into two halves and direct the flow to both hotspots

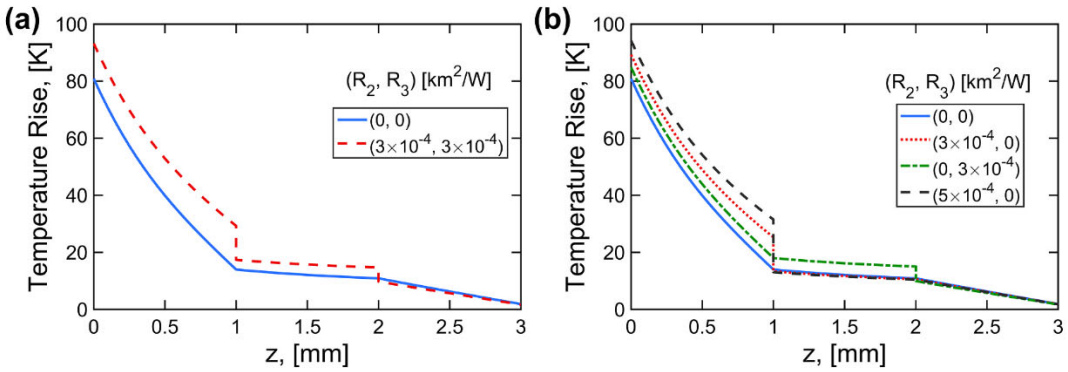

Fig. 9. Effect of inter-die thermal contact resistances: Comparison of temperature distribution as a function of z at $x = 0.003$ m with and without inter-layer thermal contact resistances for a three-layer body.

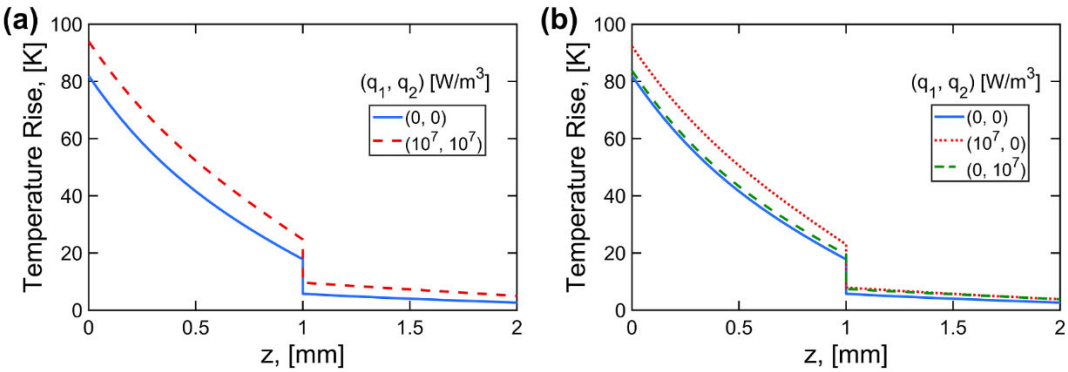

Fig. 10. Effect of internal heat generation: Comparison of temperature distribution as a function of z at $x = 0.003$ m with and without internal heat generation for a two-layer body.

(Case C). A final option considered here is to direct the entire flowrate at a location between and equidistant from the centers of the two hotspots (Case D). Temperature distribution for each case is determined using the analytical solution. Heat flux and width of each hotspot is taken to be 10^5 W/m^2 and $b = 1.0$ mm, respectively. The convective heat transfer coefficient parameters are $d = 0.5$ mm and $\gamma = 2.0$. h_{max} and h_{min} are taken to be 5000 and 500 W/m^{2}K, respectively for the full-strength jet – these values are scaled down when considering two jets, assuming constant total coolant flowrate. Thermal conductivities of the two layers are 1 and 10 W/mK, respectively, while the thickness of each layer is 1 mm. Fig. 8(a) and (b) plot the temperature distribution on the bottom and top faces, respectively, for the four cases outlined above. These Figures show that when only one hotspot is targeted with a full-strength jet (Cases A and B), there is significantly reduced temperature at the location of the targeted hotspot, but not the other hotspot. This is particularly evident from Fig. 8(b). Targeting a location between the centers of the two hotspots (Case D) is found to be an ineffective strategy, even with a full-strength jet, as it fails to reduce peak temperature of either hotspot. On the other hand, splitting the jet into two halves and directing each of the half-strength jets to the hotspots (Case C) appears to be effective in reducing the temperatures of both hotspots simultaneously, resulting in the lowest peak temperatures for both hotspots amongst the four cases considered here. While the nature of these results clearly depends on the specific values considered for the various parameters, Fig. 8 demonstrates the capability of the analytical solution presented in this work to carry out rapid thermal characterization of various possible configurations when optimizing the thermal management of a multi-layer stack, particularly in complicated scenarios, such as the presence of spatially varying heat transfer coefficient.

3.4. Impact of inter-die thermal contact resistance

The impact of inter-die thermal contact resistance is investigated. For this purpose, a three-layer body is considered, with the same parameters as Fig. 2. Fig. 9(a) plots the temperature distribution along z at $x = 3.0$ mm with perfect contact between the layers, and with a thermal contact resistance of 3×10^{-4} Km^2/W between adjacent layers. As expected, results show continuous temperature distribution in case of perfect contact, and temperature discontinuity between layers when thermal contact resistance is modeled. Due to the thermal contact resistance, the temperature distribution in the latter case is greater in the first and second layers, while there is minimal impact on the third layer.

To investigate this further, Fig. 9(b) plots the temperature distribution for a few additional cases. A non-zero value of thermal contact resistance between the first and second layers, R_2, causes an increase in temperature in the first layer compared to the baseline case of zero thermal contact resistance. The greater the value of R_2, the larger is the increase in temperature in the first layer, but there is no increase in temperature in the second or third layers. On the other hand, when a non-zero thermal contact resistance, R_3, is considered between the second and third layers, there is additional temperature rise in both first and second layers. This is because R_2 influences the thermal resistance from only the first layer to the cooling boundary. On the other hand, R_3 influences the thermal resistance from the first and second layers to the cooling boundary, but not so for the third layer. Fig. 9(b) also confirms that the larger the thermal contact resistance, the larger is the additional temperature rise.

3.5. Impact of internal heat generation rate

The impact of internal heat generation in a two-layer body is investigated. Thermal conductivity of the two layers is 1 and 10 W/mK,

respectively. Each layer is 1 mm thick. Thermal contact resistance of 3×10^{-4} Km^2/W is considered between layers. Heat flux and convective heat transfer coefficient distributions on the bottom and top faces, respectively, are the same as Fig. 2. Fig. 10(a) plots the temperature distribution along z at $x = 3.0$ mm for the baseline case of zero internal heat generation and a case where both layers generate 10^7 W/m^3 heat. Fig. 10(a) clearly shows elevated temperature distribution when internal heat generation is present. The change in temperature with respect to the baseline is greater for the first layer than the second due to the larger thermal resistance between the first layer and the cooling boundary than the second layer. In both cases, there is a temperature discontinuity at the interface, consistent with the thermal contact resistance between layers.

Fig. 10(b) investigates the impact of heat generation rate further, by considering cases of heat generation only in individual layers. When heat generation occurs only in the first layer, there is greater temperature rise in both layers compared to the baseline case of zero heat generation. The influence on temperature in the first layer is greater than on temperature in the second layer. On the other hand, when heat generation occurs only in the second layer, the additional temperature rise in both layers is about the same, and is lower than the first case. This likely occurs because heat generation in the second layer is dissipated more effectively than in the first layer and also because of the relatively lower thermal conductivity of the first layer.

4. Conclusions

Spatial variation in convective heat transfer coefficient occurs in many engineering applications, such as jet impingement cooling, due to spatial changes in the velocity field of the cooling fluid. It is important to account for these variations in analytical solutions for thermal conduction in multilayer bodies, since the assumption of constant convective heat transfer coefficient, while simplifying analysis, may lead to significant errors. This paper presents an analytical solution to account for a spatially varying convective heat transfer boundary condition in a multilayer body. To do so, the method expresses the multilayer temperature distribution as a Fourier series, the coefficients of which are chosen in order to satisfy the various boundary conditions. Specifically, the spatially varying convective boundary condition is shown to result in a set of linear algebraic equations that can be solved to determine the unknown coefficients. The theoretical solution presented here may help improve our understanding of thermal conduction in multilayer bodies. For example, the impact of variation in the heat transfer coefficient as well as various other thermal properties on the temperature distribution can be easily determined using the analytical model. Such parametric studies can be run much faster with the analytical model compared to finite-element simulations. It is expected that this may be of use in several practical engineering applications in thermal management.

Credit author statement

Long Zhou – Methodology, Formal analysis, Investigation, Data curation, Visualization; Mohammad Parhizi – Formal analysis, Data curation, Visualization; Ankur Jain – Conceptualization, Methodology, Supervision, Project administration, Data curation, Visualization. All authors contributed towards writing original draft and review/editing.

Declaration of competing interest

The authors declare that they have no known competing financial interests or personal relationships that could have appeared to influence the work reported in this paper.

Acknowledgments

This material is based upon work supported by CAREER award no. CBET-1554183 from the National Science Foundation. This research was supported by the Key Project of Science of the Education Bureau of Henan Province (19B460005), Special Project of Basic Scientific Research Operating Expenses of Henan Polytechnic University (NSFRF180427), and China Scholarship Council.

References

[1] D.W. Hahn, M.N. Özişik, Heat Conduction, third ed., John Wiley & Sons, Hoboken, New Jersey, 2012.
[2] L. Choobineh, A. Jain, An explicit analytical model for rapid computation of temperature field in a three-dimensional integrated circuit (3D IC), Int. J. Therm. Sci. 87 (2015) 103–109.
[3] K. Banerjee, S.J. Souri, P. Kapur, K.C. Saraswat, '3-D ICs, A novel chip design for improving deep-submicrometer interconnect performance and systems-on-chip integration, Proc. IEEE 89 (2001) 602–633.
[4] S. Pozder, et al., '3D Die-To-Wafer Cu/Sn Microconnects Formed Simultaneously with an Adhesive Dielectric Bond Using Thermal Compression Bonding,' 2008 International Interconnect Technology Conference, Burlingame, CA, USA, 2008, pp. 46–48.
[5] S.G. Kandlikar, Review and projections of integrated cooling systems for three-dimensional integrated circuits, 024001:1-11, ASME J. Electron. Packag. 136 (2014).
[6] F. de Monte, An analytic approach to the unsteady heat conduction processes in one-dimensional composite media, Int. J. Heat Mass Tran. 45 (2002) 1333–1343.
[7] Y. Sun, I.S. Wichman, On transient heat conduction in a one-dimensional composite slab, Int. J. Heat Mass Tran. 47 (2004) 1555–1559.
[8] L. Zhou, M.L. Bai, W.Z. Cui, J.Z. Lü, Theoretical solution of transient heat conduction problem in one-dimensional multilayer composite media, J. Thermophys. Heat Tran. 31 (2017) 481–486.
[9] I.R. Maestre, P.R. Cubillas, L. Pérez-Lombard, 'Transient heat conduction in multi-layer walls: an efficient strategy for Laplace's method, Energy Build. 42 (2010) 541–546.
[10] B. Yang, S. Liu, Closed-form analytical solutions of transient heat conduction in hollow composite cylinders with any number of layers, Int. J. Heat Mass Tran. 108 (2017) 907–917.
[11] S. Singh, P.K. Jain, Rizwan-uddin, Finite integral transform method to solve asymmetric heat conduction in a multilayer annulus with time-dependent boundary conditions, Nucl. Eng. Des. 241 (2011) 144–154.
[12] M.N. Özişik, R.L. Murray, On the solution of linear diffusion problems with variable boundary condition parameters, ASME J. Heat Transfer 96 (1974) 48–51.
[13] D. Schumayer, T.C.A. Molteno, Heat conduction in multi-layer circuit elements, in: IEEE SENSORS Conference, Busan, S. Korea, 2015, pp. 1–4.
[14] P. Biswas, S. Singh, H. Bindra, Homogenization of time dependent boundary conditions for multi-layer heat conduction problem in cylindrical polar coordinates, Int. J. Heat Mass Tran. 129 (2019) 721–734.
[15] L. Choobineh, A. Jain, Analytical solution for steady-state and transient temperature field in vertically integrated three-dimensional integrated circuits (3D ICs), IEEE Trans Components, Packaging & Manufacturing Technologies 2 (12) (2012) 2031–2039.
[16] A. Haji-Sheikh, J.V. Beck, Temperature solution in multi-dimensional multi-layer bodies, Int. J. Heat Mass Tran. 45 (2002) 1865–1877.
[17] J. Geer, A. Desai, B. Sammakia, Heat conduction in multilayered rectangular domains, ASME J. Electron. Packag. 129 (2007) 440–451.
[18] T.L. Bergman, D.P. Dewit, A.S. Lavine, F.P. Incropera, Fundamentals of Heat and Mass Transfer, John Wiley & Sons, New Jersey, 2011.
[19] R.J. Goldstein, A.I. Behbahani, K.K. Heppelmann, Streamwise distribution of the recovery factor and the local heat transfer coefficient to an impinging circular air jet, Int. J. Heat Mass Tran. 29 (1986) 1227–1235, https://doi.org/10.1016/0017-9310(86)90155-9.
[20] S.W. Ma, A.I. Behbahani, Y.G. Tsuei, Two-dimensional rectangular fin with variable heat transfer coefficient, Int. J. Heat Mass Tran. 34 (1991) 79–85.
[21] D. Sarkar, A. Jain, R. Goldstein, V. Srinivasan, Corrections for lateral conduction error in steady-state heat transfer measurements, Int. J. Therm. Sci. 109 (2016) 413–423.
[22] D. Sarkar, K. Shah, A. Haji-Sheikh, A. Jain, Analytical modeling of temperature distribution in an anisotropic cylinder with circumferentially-varying convective heat transfer, Int. J. Heat Mass Tran. 79 (2014) 1027–1033.
[23] D. Sarkar, A. Haji-Sheikh, A. Jain, Thermal conduction in an orthotropic sphere with circumferentially varying convection heat transfer, Int. J. Heat Mass Tran. 96 (2016) 406–412.
[24] S. Luhar, D. Sarkar, A. Jain, Steady state and transient analytical modeling of non-uniform convective cooling of a microprocessor chip due to jet impingement, Int. J. Heat Mass Tran. 110 (2017) 768–777.
[25] L. Zhou, M. Parhizi, A. Jain, Temperature distribution in a multi-layer cylinder with circumferentially-varying convective heat transfer boundary conditions, 106673:1-12, Int. J. Therm. Sci. 160 (2021).
[26] R.L. McMasters, F. de Monte, J.V. Beck, D.E. Amos, Transient two-dimensional heat conduction problem with partial heating near corners, 021301:1-10, ASME J. Heat Transfer 140 (2018).
[27] L. Choobineh, J. Jones, A. Jain, Experimental and numerical investigation of interdie thermal resistance in three-dimensional integrated circuits, 020908:1-6, J. Electron. Packag. 139 (2017).